Transition from Bohm to classical diffusion due to edge rotation of a cylindrical plasma

J. E. Maggs, T. A. Carter, and R. J. Taylor
Physics and Astronomy Department, University of California, Los Angeles, Los Angeles, California 90095

The outer region of the plasma column of a large, linear plasma device is rotated in a controlled fashion by biasing a section of the vacuum chamber wall positive with respect to the cathode ($E_r < 0$). The magnitude and temporal dependence of the observed cross-field current, produced when the bias voltage is applied, is consistent with ion current arising from ion-neutral collisions. Flow speeds in the outer regions of the plasma column exceed the local sound speed. In the nonrotating plasma column, cross-field, radial particle transport proceeds at the Bohm diffusion rate. Rotation, above a threshold bias voltage, reduces cross-field transport from Bohm to classical rates, leading to steeper radial density profiles. Reduction of particle transport is global and not isolated to the region of flow shear. The transition from the nonrotating to the rotating plasma edge in the linear plasma column is similar to the low confinement to high confinement mode transition observed in tokamaks when $E_r < 0$. © 2007 American Institute of Physics. [DOI: 10.1063/1.2722302]

I. INTRODUCTION

A key advance in the art of plasma confinement by magnetic fields is the discovery that cross-field bulk plasma flow leads to reduced cross-field particle transport.[1,2] Poloidal flows in tokamaks are involved in the low confinement (L) mode to high confinement (H) mode transition.[3] The L mode is characterized by density profiles with gentle gradients while the H mode is characterized by profiles with steep gradients.[4] The difference in profile shape is believed to be caused by a so called "transport barrier" arising from the suppression of turbulent transport due to poloidal flow and flow shear.[5,6] Poloidal flows can arise from externally applied biases[7] or from internally driven processes (e.g., zonal flows[8]).

An important question to answer is what physical mechanisms are involved in the change of particle transport in the presence of plasma flow?[9,10] To answer this question, it is useful to have some idea of what processes are involved in particle transport in the absence of flow.[11] Cross-field particle transport is believed to arise from diffusive or fractionally diffusive processes,[12] and thus inherently involves a decorrelation process either associated with collisions or wave-particle interactions. In tokamaks, diffusive processes are dominated by plasma wave turbulence, and the key question becomes, what modes are involved in the turbulence that drives particle transport?[13] Diffusive processes, of necessity, occur in regions of cross-field plasma pressure gradients. These same gradients are sources of free energy that can drive drift modes,[14] and it is natural to investigate the role of these modes in particle transport. Once the modes involved in transport in the flow-free plasma are identified, the question of how flow effects the mode structure, mode decorrelation,[15] and the growth rates of primary and secondary instabilities[16] can be addressed.

The results reported here are from experiments conducted in the upgraded version of the Large Plasma Device [LAPD (Ref. 17)] operated under the auspices of the Basic Plasma Science Facility (BaPSF) at the University of California at Los Angeles (UCLA). The magnetized, cylindrical plasma column of the LAPD is 17.6 m long and 60 cm in diameter. In large magnetized plasmas, drift modes couple with the shear Alfvén wave to become drift-Alfvén waves,[18] and these are the dominant low-frequency, long parallel-wavelength modes spontaneously generated by cross-field plasma pressure gradients. The LAPD plasma column is long enough to support drift-Alfvén wave turbulence.[19] Therefore, it is of broad interest to study the properties of cross-field particle transport and the effects of rotation on transport in the simple, linear magnetic geometry of the plasma column of the LAPD because the complicating effects of magnetic field-line curvature, poloidal asymmetry, and trapped particle orbits are absent.

This paper reports on the general properties of radial particle transport in the LAPD. Details of turbulence and turbulence structure are reported in a companion paper. Evidence is presented that the radial density profiles of the non-rotating plasma column in the LAPD are produced by Bohm diffusion. Plasma rotation reduces radial particle transport to classical rates and results in density profiles with steep radial gradients. Changes in electron heat transport are not investigated in this study.

The transition is reminiscent of the L to H mode transition observed in tokamaks, in that azimuthal (poloidal) rotation reduces radial particle transport by large amounts. In these experiments conducted in the LAPD, azimuthal flows arise due to cross-field ion currents that lead to radial electric fields. These currents arise from ion-neutral collisions and provide the torque needed to rotate the plasma. The reduction of radial particle transport is global and not isolated to the region of flow or flow shear.
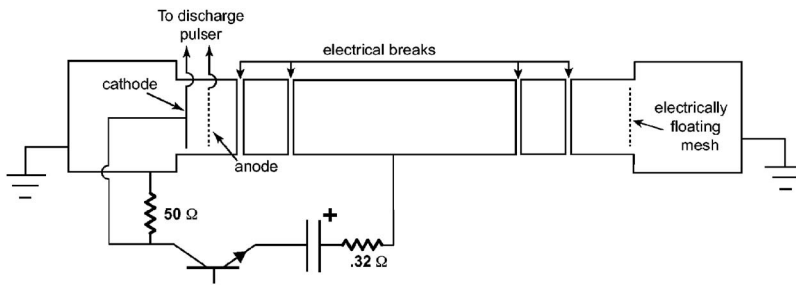
14, 052507-1

FIG. 1. A schematic of the experimental setup. A voltage bias pulse is applied between the cathode and the electrically floating, central section of the vacuum chamber wall. The magnetic field is uniform, and the plasma column is terminated by an electrically floating grid. Ion current flows across the magnetic field from the wall to the cathode, producing a torque that spins up the outer edge of the plasma column.

II. EXPERIMENTAL SETUP

Figure 1 is a schematic drawing of the arrangement used to induce rotation in the edge of the LAPD plasma column. The LAPD device produces plasma using 40–60 V electrons created by pulsing a barium-oxide coated cathode negative with respect to a mesh anode located about 50 cm away. The fast electrons ionize helium gas at a fill pressure of 10^{-4} Torr, creating a plasma with 6–8 eV electron temperature, about 1 eV ion temperature, and density in the range $(2-4)\times10^{12}$ cm^{-3}. The cathode-anode arrangement is located at one end of the plasma column. The vacuum chamber of the LAPD is 22 m in overall length, consisting of two end chambers 1.52 m in diameter and a central section, containing the plasma column, 1.0 m in diameter. The LAPD plasma column is 17.6 m in length and 60 cm in diameter. The central vacuum chamber consists of several segments, which can be electrically isolated from each other and ground. The plasma column is terminated with an electrically floating mesh.

The plasma rotation circuit consists of a 500 V, 2500 A transistor switch, 0.2 Farad, 500 V capacitor bank, and 0.32 Ω current limiting resistor connected as shown in Fig. 1. The rotation bias is pulsed on for 4 ms during the main plasma discharge, which is typically 10 ms long. The positive side of the capacitor bank is connected to a 10-m-long central section of the vacuum chamber, which is electrically isolated from the neighboring sections and ground. The sections immediately adjacent to the central section are also electrically isolated. Both end chambers with an attached segment of plasma chamber are grounded. The collector of the transistor is connected to the cathode. A 50 Ω resistor keeps the cathode potential near ground.

When the bias pulse is applied, current flows across the magnetic field from the chamber wall to magnetic field lines connected to the cathode. The $J\times B$ torque associated with the cross-field current spins up the tenuous "halo-plasma" in the region between the edge of the cathode and the chamber wall. A steady state with rotating halo-plasma, radial electric field, and cross-field current is reached in about 2 ms.

III. NEUTRALS

Ion-neutral collisions are potentially important because they provide a mechanism for driving ion currents across the magnetic field. In order to judge their importance, knowledge of the spatial and temporal behavior of the neutral gas during the plasma discharge is needed. Direct measurements of the neutral gas behavior are not available, so it is neces-

sary to construct a dynamic model of the neutral density. The electron temperature in the LAPD plasma is high enough to lead to significant ionization once the plasma is formed, so the neutral density is closely coupled with the plasma density. The equations governing the temporal evolution of the neutral and plasma densities, n_0 and n, are

$$\frac{\partial n_0}{\partial t} + \nabla \cdot \Gamma_0 = S_0 - L_0, \tag{1a}$$

$$\frac{\partial n}{\partial t} + \nabla \cdot \Gamma_e = S_e - L_e. \tag{1b}$$

Γ_0 and Γ_e are, respectively, the neutral and electron particle fluxes, S_0 and S_e the particle sources, and L_0 and L_e the particle sinks. The ions and electrons are assumed to move together, so the plasma density and plasma particle flux are taken to be the same as the electron density and electron flux.

Neutrals are fed into the LAPD by a voltage-controlled piezoelectric valve located near the center of the main vacuum chamber. The throughput of the LAPD vacuum pumping system is about 3×10^{19} particles/s at the neutral fill pressure of 10^{-4} Torr. In the steady-state operation of the LAPD, the neutral source associated with the piezoelectric valve balances this pumping speed. This source strength is several hundred times smaller than the volume production rate of plasma and subsequent reduction of neutrals during the plasma discharge and thus it need not be included in the source term of Eq. (1a) when discussing the neutral behavior during the discharge. The other possible sources for neutrals are recombination and recycling from the chamber walls. Recombination need not be included in the source term of Eq. (1a) because recombination rates[20] are much longer than the discharge pulse length at electron temperatures and densities common to the LAPD discharge plasma. The neutral recycling rate is taken to be equal to the plasma loss rate at the vacuum chamber walls ($S_0=L_e$).

The sink for neutrals is ionization caused by both the fast electrons from the cathode and the tail particles in the thermal distribution of the bulk plasma. The sink for neutrals is equal to the source for plasma ($S_e=L_0$). As mentioned above, plasma is lost when it contacts the chamber wall.

To proceed further, two simplifications are used. All quantities are assumed to be azimuthally symmetric, and the axial variation (along the magnetic field) of neutral and plasma density is ignored, but the machine is assumed to have finite length. Using these simplifications, adding Eq.

(1a) to Eq. (1b), and integrating over the chamber volume gives

$$\int \left[\frac{\partial n_0(r,t)}{\partial t} + \frac{\partial n(r,t)}{\partial t} \right] dV + [\Gamma_{0,r}(R) + \Gamma_{e,r}(R)]4\pi RL$$
$$+ 2[\Gamma_{0,z}(L) + \Gamma_{e,z}(L)]\pi R^2 = 0. \qquad (2)$$

In Eq. (2), $2L$ is the length, and R is the radius of the plasma chamber. The quantity $\Gamma_{0,r}(R)$ is the radial neutral flux, and $\Gamma_{e,r}(R)$ is the radial electron flux, evaluated at the chamber wall. Similarly, $\Gamma_{0,z}(L)$ and $\Gamma_{e,z}(L)$ are the axial fluxes evaluated at the ends of the machine. Equation (2) is used to relate the plasma density to the neutral density to obtain a single equation for the evolution of the neutral particle density.

To construct a model of the behavior of the neutral particle density in the LAPD, it is convenient to begin by considering the ionization processes occurring on a single field line in the presence of a stationary (i.e., zero velocity, $\Gamma_0 = 0$) neutral population and no plasma losses ($\Gamma_e = 0$). Ionization of neutrals occurs due to two separate electron populations, the monoenergetic electrons emitted from the cathode (the so called "beam" electrons) and the thermal electrons in the bulk plasma. Both electron population densities are functions of time, with the temporal duration of the beam population under the external control of the experimenter. The ionization process is assumed to produce a single electron and a single ion. The ionization rate due to a single beam electron is $R_b = \sigma(E_b)v_b$, where E_b is the beam energy, v_b is the beam velocity, and $\sigma(E)$ is the ionization cross section at energy E. The ionization rate due to all beam electrons is $S_b = R_b n_b$, where n_b is the number density of beam electrons. The beam density is known from measurements of the discharge current and voltage. The beam density is typically small compared to the plasma density and it is not included in the bulk plasma population in these calculations. The ionization rate due to the thermal population of plasma electrons is $R_p = \langle \sigma(T_p)v \rangle$, where the angular brackets denote an average over the velocity distribution of the thermal population with temperature, T_p. The ionization rate due to all plasma electrons is then $S_p = R_p n$, where n is the number density of the thermal plasma electrons. The values of both $\sigma(E)$ and R_p are readily available from published data.[21]

The temporal rate of change in the neutral density from Eq. (1b) is then

$$\frac{\partial n_0(t)}{\partial t} = -L_0 = -S_b n_0(t) - R_p n_0(t)n(t). \qquad (3)$$

Since we are considering the ionization processes occurring on a single field line in the absence of particle fluxes, Eq. (2) can be written as $\partial n/\partial t + \partial n_0/\partial t = 0$, or

$$n(t) = n_0(0) - n_0(t), \qquad (4)$$

where $n_0(0)$ is the initial neutral density. Using this relation in Eq. (3) results in

$$\frac{\partial \ln[n_0(t)]}{\partial t} = -S_b(t) - R_p n_0(0) + R_p n_0(t). \qquad (5)$$

The solution to Eq. (5) is

$$n_0(t) = \frac{n_0(0)A(t)}{1 - n_0(0)R_p \int_0^t A(t')dt'};$$
$$A(t) = \exp\left\{ -\int_0^t [S_b(t') + R_p n_0(0)]dt' \right\}, \qquad (6)$$

as can be verified by direct substitution. Equation (6) can be used to determine the temporal evolution of the neutral density and plasma density on a single field line.

The behavior across a diameter of the actual machine can be found by allowing the beam ionization rate to be a function of position, $S_b(t) \rightarrow S_b(r,z,t)$. To simplify things, consider a slab model in which the axial variation can be ignored, and reduce the spatial dependence to one dimension across the plasma column. With the spatial dependence of the source specified, $S_b(x,t)$, Eq. (6) gives the spatial and temporal evolution of the neutral density, $n_0(x,t)$, for each field line. With the assumption that electrons created by ionization are tied to the field lines on which they are created (i.e., ignoring cross-field diffusion), so that field lines evolve independent of each other, Eq. (2) has the solution $n(x,t) = n_0(0) - n_0(x,t)$. The expression for the plasma density obtained under these assumptions is valid only if the neutrals and plasma do not move across the field.

To consider the case in which the neutrals are moving (in the radial direction only), we note that the mean free path length of neutrals at 10^{-4} Torr is about 60 cm, the width of the LAPD plasma column, so we treat them as ballistic particles. It is also convenient to first consider the case of a single velocity and then generalize to the case of a distribution of velocities. For the case in which the neutral velocity is v_0, it is useful to change variables from (x,t) to (w,z), where

$$z = \left(t + \frac{x}{|v_0|} \right), \quad w = \left(t - \frac{x}{|v_0|} \right), \quad t = z + w,$$
$$x = (z - w)|v_0|, \quad \frac{\partial}{\partial t} \rightarrow \frac{\partial}{\partial t} + v_0 \frac{\partial}{\partial x}. \qquad (7)$$

Equation (1a) then becomes

$$\frac{\partial \tilde{n}_0(z,w)}{\partial z} = -\tilde{S}_b(z,w)\tilde{n}_0(z,w) - R_p\tilde{n}_0(z,w)\tilde{n}(z,w), \qquad (8)$$

where

$$\tilde{n}(z,w) = n((z-w)|v_0|, z+w) = n(x,t). \qquad (9)$$

Equation (8), which is for right-going (i.e., w=const) particles, has a companion equation for left-going (i.e., z=const) particles. The solution for right-going particles is

$$\ln n_{0r}(z,w,v_0) = -\int_{-w}^{z} [\tilde{S}_b(z',w) + R_p\tilde{n}(z',w)]dz', \qquad (10)$$

with a similar expression for left-going particles in which the integration is over the variable, w, while z is held constant. In integrating Eq. (8), neutral particles are assumed to specu-
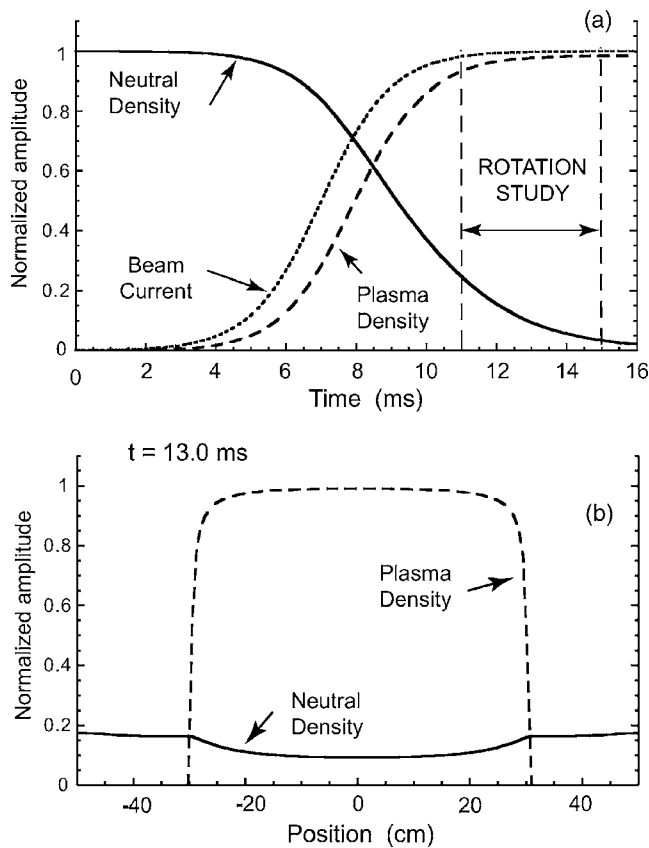
FIG. 2. (a) The predicted temporal behavior of the neutral helium density and the plasma density at the center of the plasma column from a model that does not include plasma losses. The neutral density is normalized to 3 $\times 10^{12}$ cm^{-3} and the plasma density to 5×10^{12} cm^{-3}. The temporal behavior of the discharge beam current is an input to the model. The rotation bias pulse is applied near the end of the discharge in the region marked "rotation study." This model predicts a neutral density below 30% of its starting value. (b) The predicted profile of the neutral and plasma densities across the plasma column 13 ms after the initiation of the ionizing beam current. The increase in neutral density near the walls arises from very slow neutrals that are encountering the wall for the first time. Neutrals with velocities above half the thermal speed have flat profiles across the column.

larly reflect off the walls of the vacuum chamber. The technique for solving Eq. (10) is iterative. In the first iteration, the expression for the electron density obtained under the assumption of stationary neutrals and no particle losses is used. This approach assumes that the ionization time is shorter than the time it takes a neutral to traverse the plasma column. This is true only for the slower moving neutrals. Furthermore, in the results presented in Fig. 2, only one iteration is used in the solutions.

The final expression for the neutral density is then obtained by adding the contributions of left- and right-going particles,

$$n_0(z,w,v_0) = \frac{1}{2}\{\tilde{n}_{0r}(z,w,v_0) + \tilde{n}_{0l}(z,w,v_0)\}. \quad (11)$$

The neutral density behavior for a thermal distribution of neutral particles can be found by using Eq. (11) for N discrete values of velocity, v_{0i}, and summing the resulting neutral density profiles, $n_0(z,w,v_{0i})$, weighted with the velocity distribution profile $f_0(v_{0i})$, where f_0 is a Maxwellian distri-

bution at room temperature with thermal velocity $v_{0\text{th}}=7.8 \times 10^4$ cm/s,

$$\tilde{n}_0(z,w) = \sum_0^N f_0(v_{0i})n_0(z,w,v_{0i}). \quad (12)$$

The predictions of the neutral model are shown in Fig. 2. Figure 2(a) shows the temporal evolution of the plasma density and neutral density at the center of the plasma column. The electron temperature is 7.0 eV and is assumed constant across the plasma column. The neutral density is normalized to a value of 3.0×10^{12} cm^{-3} and the plasma density is normalized to a value of 5.0×10^{12} cm^{-3}. The temporal form of the discharge current, obtained from measurements, is an input to the model, and is shown as well. The discharge current is normalized to a value of 4000 Amps. In the experiments, the rotation bias is applied to the plasma during a 4 ms period near the end of the discharge pulse. The location of this time interval in the neutral model is denoted as "rotation study." Figure 2(b) shows a radial profile of the neutral density, and the plasma density, corresponding to a time of 13 ms in Fig. 2(a). The slight rise in neutral density outside the plasma column results from very slow neutrals that have moved out of the central plasma column. The radial profile of neutrals with velocities greater than about half the thermal speed is essentially flat. In constructing the neutral profile, nine discrete velocity bins were used; the first centered at $v_0=0.0625\ v_{0\text{th}}$ with width $v_{0\text{th}}/8$, and the remaining eight bins of width $v_{0\text{th}}/4$ centered at $0.25\ v_{0\text{th}}$, $0.5\ v_{0\text{th}}$, etc. The neutral model predicts that, during the period of plasma rotation, the neutral fraction is between 10 to 20%, and the profile is nearly constant across the plasma column.

This model of neutral evolution ignores both radial and axial plasma losses and thus greatly overestimates the rate of neutral depletion and the final plasma density. An improved model of the temporal evolution of both the neutral and plasma density is obtained by including losses due to plasma particle transport. In the particle transport model, a detailed study of the radial dynamics of the neutrals is not included. Rather, the lessons learned from the neutral model are incorporated by assuming that the neutral density profile is constant across the plasma column.

IV. PLASMA PARTICLE TRANSPORT

Equation (1b) determines the behavior of the plasma density. It can be written (assuming azimuthal symmetry) as

$$\frac{\partial n(t)}{\partial t} + \nabla \cdot \Gamma_e = \frac{\partial n(t)}{\partial t} + \nabla_r \cdot \Gamma_{e,r} + \frac{\partial \Gamma_{e,z}}{\partial z}$$
$$= S_e = S_b n_0(t) + R_p n_0(t)n(t), \quad (13)$$

where $\Gamma_{e,r}$ and $\Gamma_{e,z}$ are the particle fluxes in the radial and axial directions, respectively. S_e is the plasma production rate as discussed above in connection with the neutral model. From the force balance equations for the electron and ion fluids, the particle flux in the radial direction resulting from transport due to Coulomb collisions (classical transport) is found to be[22–24]

$$\Gamma_{e,r} = -\frac{c}{eB} \left\{ \frac{\nu_F}{\Omega_e} \frac{\partial p}{\partial r} - \frac{3}{2} \frac{\nu_T}{\Omega_e} n \frac{\partial T_e}{\partial r} \right\}, \tag{14}$$

where ν_F is the collision frequency associated with the frictional force, and ν_T is the collision frequency associated with the thermal force. For classical transport, $\nu_F = \nu_T = \nu_{ei}$, where ν_{ei} is the electron-ion collision rate due to Coulomb interactions, $\nu_{ei} = 2.9 \times 10^{-6} \, n\Lambda/T_e^{3/2}$, with Λ the Coulomb logarithm. To allow for the possibility of anomalous, or nonclassical, transport, the collision frequencies in Eq. (14) are written in a generalized form.

The total plasma pressure is denoted by $p = n(T_i + T_e)$, where T_i is the ion temperature and T_e the electron temperature. In the LAPD, the ion temperature is much smaller than the electron temperature ($T_i \ll T_e$), so the plasma pressure can be written as $p = nT_e$. The radial particle flux then has the form

$$\Gamma_{e,r} = -D_F \frac{\partial n}{\partial r} - D_T n \frac{\partial \ln(T_e)}{\partial r}, \tag{15}$$

where the diffusion coefficients D_F and D_T are defined as

$$D_F = \frac{c}{eB} \frac{\nu_F}{\Omega_e} T_e \quad \text{and} \quad D_T = \frac{c}{eB} \left[\frac{\nu_F}{\Omega_e} - \frac{3}{2} \frac{\nu_T}{\Omega_e} \right] T_e. \tag{16}$$

Note that, if ν_F/Ω_e is taken equal to 1/16, D_F becomes the Bohm diffusion coefficient, D_B. The magnitude and sign of the diffusion coefficient D_T is determined by the details of the collision cross sections involved in the processes of slowing the bulk flow of electrons through ions (frictional force) and scattering of gyrating electrons off ions (thermal force). In particular, the negative sign of D_T arising in classical transport, that is, when $\nu_F = \nu_T = \nu_{ei}$, is due to the $1/v^3$ dependence of the Coulomb collision cross section (i.e., fast particles make fewer collisions). Collision cross sections involved in anomalous transport might be expected to result in a significant deviation of D_T from its classical value, $-D_F/2$.

The term involving axial particle flux, $\Gamma_z = nv_z$, is taken to represent loss of plasma along the magnetic field to the ends of the device. The plasma interface at the end walls of the device involves the formation of a Bohm sheath and the plasma loss rate should be proportional to the ion sound speed at the beginning of the sheath. Thus the axial loss rate term $\partial \Gamma_z / \partial z$ is taken to be n/τ_L with $\tau_L = L_c/c_s$, where L_c is a characteristic length and c_s is the ion sound speed, $c_s = (T_e/M)^{1/2}$, at the center of the plasma column. The appropriate value of the end loss rate can be found by comparing the rise time of the measured plasma-discharge current to the plasma density as discussed below.

The plasma production rate, $S_b n_0 + R_p n_0 n$, depends on the neutral density, n_0. As mentioned earlier, the radial profile of the neutral density is assumed constant in this model. The temporal behavior of the neutral density is obtained from the temporally evolving plasma density by using Eq. (2). Recall that it is assumed that the ionization process produces a single electron and ion, and that any plasma lost to the walls is immediately recycled into neutral particles [$\Gamma_{0,r}(R) + \Gamma_{e,r}(R) = 0$ and $\Gamma_{0,z}(L) + \Gamma_{e,z}(L) = 0$]. Equation (2) becomes

$$\int_0^R \left[\frac{\partial n_0(r,t)}{\partial t} + \frac{\partial n(r,t)}{\partial t} \right] r dr$$

$$= \frac{R^2}{2} \frac{\partial n_0(t)}{\partial t} + \int_0^R \left[\frac{\partial n(r,t)}{\partial t} \right] r dr = 0. \tag{17}$$

The spatial integration over the neutral density is trivial because the neutral profile is assumed constant. A discrete form of Eq. (17) is used to temporally evolve the neutral particle density. At each time step, t_k, the change in neutral density is obtained by radial integration of the change in plasma density,

$$n_0(t_k) = n_0(t_{k-1}) - \frac{2}{R^2} \int_0^R [n(t_k) - n(t_{k-1})] r dr. \tag{18}$$

Using the expressions for $\Gamma_{e,r}$ and $\partial \Gamma_{e,z}/\partial z$, the equation governing radial plasma dynamics in the LAPD is

$$\frac{\partial n}{\partial t} - \frac{1}{r} \frac{\partial}{\partial r} r D_F \frac{\partial n}{\partial r} - \frac{1}{r} \frac{\partial}{\partial r} r D_T n \frac{\partial \ln(T_e)}{\partial r}$$

$$= S_b n_0 + R_p(T_e) n_0 n - \frac{n}{\tau_L}. \tag{19}$$

It should be noted that the plasma ionization rate, R_p, is a sensitive function of temperature, and this dependence is included in the calculation of the production rate. In using Eq. (19) to solve for the plasma density profile, the electron temperature profile is assumed known. In practice, the measured electron temperature profile is used to evaluate the terms in Eq. (19) containing the temperature and its radial derivative. Equation (19) can be numerically solved using the tridiagonal method. The coefficients needed to implement the tridiagonal solution are given in the Appendix.

Note that, in the absence of axial and radial losses, the only steady-state solution to Eq. (19) is $n_0 = 0$, i.e., complete burnout. On the other hand, with particle losses, the neutral recycling assumptions embodied in Eq. (18) allow for a steady-state solution in which the neutral density is not zero. The steady-state plasma profile produces just enough ionization to balance the neutral recycling created by plasma losses to the walls. Such behavior is illustrated in Fig. 3, which should be compared to Fig. 2(a). The temporal development of the neutral and plasma density is shown at the center of the nonrotating plasma column. The neutral density is normalized to a starting density of 3.8×10^{12} cm^{-3} and the electron density is normalized to 2×10^{12} cm^{-3}. The details of obtaining the model curves are discussed in the next section. In contrast to the model with no plasma losses [Fig. 2(a)], a steady state is reached in which the neutral density is much higher during the period when the plasma is rotated (11–15 ms). The temporal evolution of the model plasma density (short-dash curve) is compared to the column-averaged density (solid curve) measured by an interferometer located near the axial center of the plasma column. The end loss rate is adjusted to give the good fit between the model curve and the observed column-averaged plasma density.
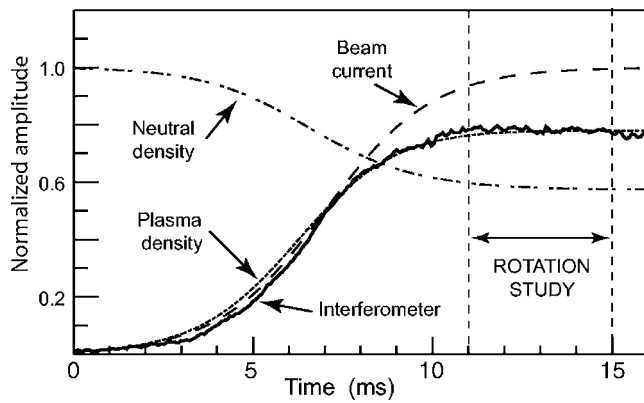
FIG. 3. The predicted temporal behavior of the neutral helium density (dot-dash curve) and the plasma density (dotted curve) at the center of the plasma column from a model that includes plasma losses. A steady state is achieved after about 12 ms. The neutral density is normalized to 3.8×10^{12} cm^{-3} and the plasma density to 2×10^{12} cm^{-3}. The dashed line (beam current) represents a fit to a measured discharge current profile. The model plasma density is compared to the column-averaged density measured by an interferometer (solid curve) located axially at the machine midpoint. The radial neutral density profile is constant across the machine in this model. In this model, the neutral density decreases to only 60% of its initial value during the time period of the rotation study.

A. The nonrotating plasma

The radial density profile of the plasma column in the LAPD is observed to change appreciably due to rotation of the edge plasma. To gain an appreciation of the change in particle transport due to rotation, an understanding of particle transport in the nonrotating plasma is essential. For this purpose, Eq. (19) is solved, together with Eq. (18), to obtain the plasma density as a function of radial position and time and the temporal evolution of the neutral density. The temporal behavior of the beam ionization term, S_b, is fit to measurements of the discharge current while the radial dependence of S_b is modeled as

$$S_b(r) = S_b(0)\{1.0 - \tanh[(r - r_s)/L_s]\}/2, \qquad (20)$$

where r_s is the radius of the beam source and L_s determines the steepness of the edge of the source. In the model profiles used for comparison with data, L_s is taken as 0.5 cm, and the beam radius, r_s, is 28.5 cm. The model plasma density profiles do not depend too sensitively on the radial profile of the ionizing beam. The edge of the plasma column moves out, if r_s is increased, and in, if r_s is decreased, but not by the same amount as the increase or decrease in r_s. The gradient scale length of the plasma edge is set by transport processes, as long as L_s is chosen shorter than the scale length set by the transport processes. The measured, radial electron temperature profile is used to evaluate terms in Eq. (19) that contain the temperature or its derivative. The radial temperature profile is measured using a triple probe. The normalized plasma density profile is obtained by dividing the ion saturation current, measured by the same probe, by the square root of the temperature.

The end loss rate term in Eq. (19), n/τ_L, is found by comparing the temporal dependence of the discharge current to the temporal dependence of the column-averaged plasma density obtained from an interferometer located at the mid-
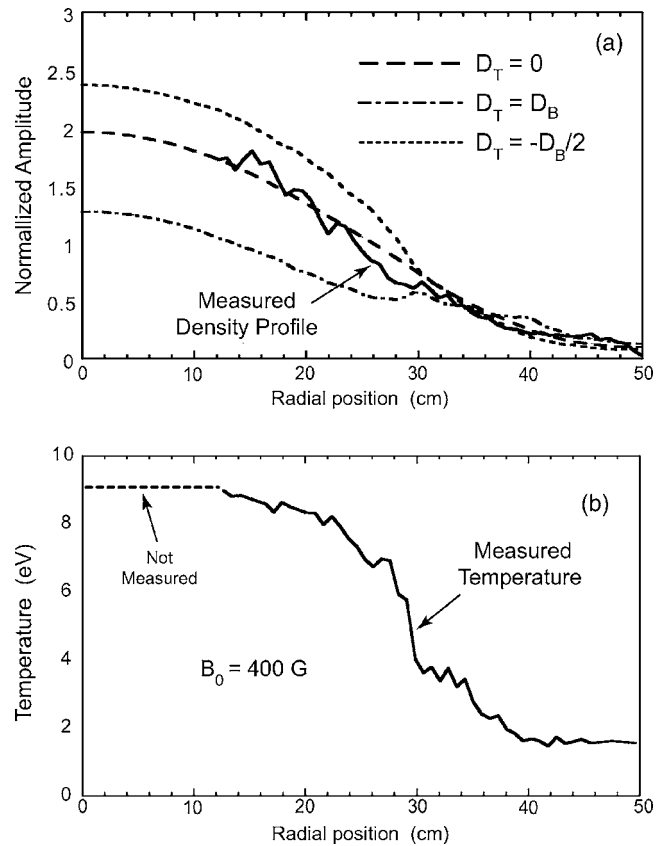

FIG. 4. (a) The plasma density profile of the nonrotating plasma column is compared to the predictions of Bohm diffusion. The solid curve is the plasma density profile derived from triple probe measurements. The dashed curve is diffusion with $D_F = D_B$ and $D_T = 0$, the situation of "pure" Bohm diffusion. The dotted curve is diffusion with $D_F = D_B$ and $D_T = -D_B/2$, and the dash-dot curve is for $D_F = D_B$ and $D_T = D_B$. The model density profiles are normalized to 2×10^{12} cm^{-3}, and the magnetic field is uniform with a strength of 400 G. The boundary conditions are set to zero radial derivative at the machine center and chamber wall. (b) The measured temperature profile used to evaluate the Bohm diffusion coefficient.

point of the plasma column. Once a plasma forms, it becomes the dominant ionization source and, thus, the temporal dependence of the plasma density is sensitive to the plasma loss rate. If the loss rate is large, the buildup of plasma density is slow compared to the buildup of the discharge current. The rise in plasma density lags well behind the rise in discharge current. In contrast, when the loss rate is small, the plasma density builds up quickly and closely follows the rise in the discharge current. Thus, the end loss rate can be determined from experimental data. The end loss rate for the results reported here is 800 s^{-1} or $\tau_L = 1.25$ ms.

It is found that particle transport at Bohm diffusion rates provides a reasonable quantitative prediction of the measured transport in the nonrotating plasma, and, therefore, this case is discussed in detail. Figure 4 shows a comparison of a measured plasma density profile to three model profiles based on Bohm diffusion. The model profiles are normalized to a value of 2×10^{12} cm^{-3}. The plasma density profile is obtained from experiments performed in an axially uniform magnetic field of 400 G. The plasma density profile is reliably determined from ion saturation measurements, but the magnitude of the density is not. In the comparisons shown
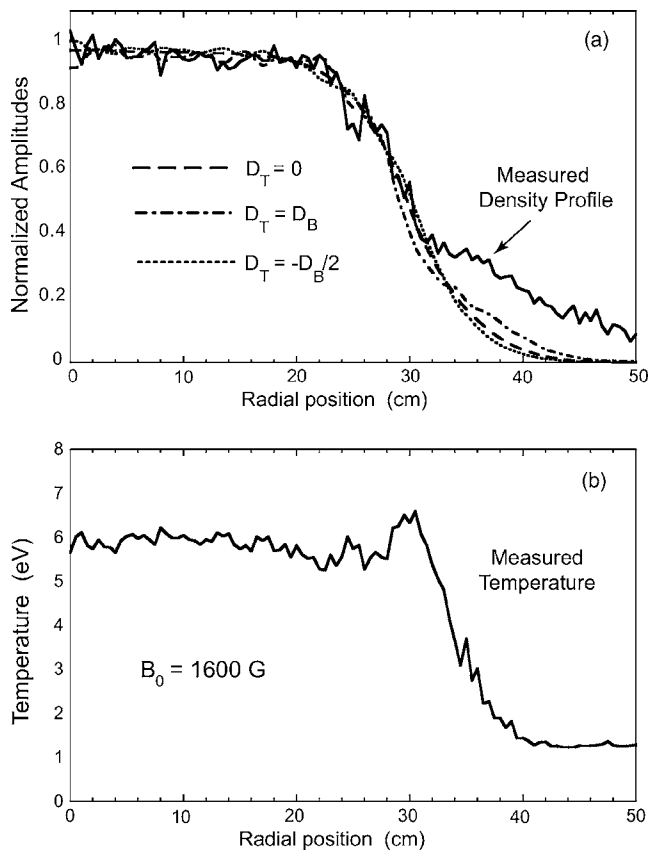
FIG. 5. Same as Fig. 4 but with a field strength of 1600 G. In this case, the plasma density is higher than predicted by the diffusion models in the region between 30 and 50 cm.

between model profiles and measured profiles, the magnitude of the plasma density is adjusted to give the best fit to model profiles.

In pure Bohm diffusion, the ratio ν_F/Ω_e is set equal to 1/16 and the diffusion coefficient D_F defined in Eq. (16) becomes the Bohm diffusion coefficient, $D_F=D_B$, while D_T is set equal to zero (which implies $\nu_F=3\nu_T/2$: $D_F=D_B$, D_T =0). The dashed curve in Fig. 4(a) is the predicted profile resulting from pure Bohm diffusion and the solid line is the measured normalized plasma density profile. The measured temperature profile used to obtain the Bohm diffusion coefficient is shown in Fig. 4(b). The boundary conditions used to obtain the model profiles are as follows: zero slope at the plasma center ($\partial n/\partial r=0$ at $r=0$), and at the chamber wall ($\partial n/\partial r=0$ at $r=r_{wall}$). Corrected Bohm diffusion is the case in which $D_F=D_B$ but D_T is not zero, so that corrections to the radial flux depending on gradients in the electron temperature are included ($D_F=D_B$, $D_T\neq0$). Profiles for two extreme values of D_T are shown. The dotted curve in Fig. 4(a) is the corrected Bohm profile for the case in which $\nu_F=\nu_T$, so that $D_T=-D_B/2$. This situation would be the same as in the case of classical diffusion, but now the diffusion coefficient is much larger than in the classical case. The dash-dot curve is the corrected Bohm profile for $\nu_T=0$, so that $D_T=D_B$. Pure Bohm diffusion ($D_F=D_B$, $D_T=0$) gives the best fit to the data.

Figure 5 shows the same curves as in Fig. 4, but for a

uniform magnetic field value of 1600 G. The Bohm diffusion rate changes by a factor of 4 from the case illustrated in Fig. 4 to the case of Fig. 5. The model profiles very clearly reproduce the observed density profile for the plasma core. However, the region near the wall ($r>35$ cm) is not represented very well in the model profiles for the 1600 G case. The origin of this behavior is not understood.

In general, the pure Bohm diffusion profile is a good estimate of the profile behavior and it is quite clear that the plasma density profile of the nonrotating plasma is determined by Bohm diffusion. Therefore, in the following, only pure Bohm diffusion profiles are used in comparing model results to observations.

B. The rotating plasma

1. Azimuthal flows

The application of a bias voltage between the chamber wall and cathode results in rotation of the outer regions of the plasma column. The sign of the applied bias is such that the chamber wall is at higher potential than the plasma. Biases of the opposite sign were tried, but resulted in escape of plasma (i.e., arcing) to the chamber wall. Plasma flow in the azimuthal and axial directions is measured using a six-faced Mach probe. The Mach probe comprises three pairs of diametrically opposed, flat, 0.75×2 mm, tantalum collecting surfaces, or faces. The normals of the collecting surfaces are oriented perpendicular to the axis of the probe shaft, which is inserted radially into the machine. The face pairs are separated by 45 degrees around the probe shaft axis. Plasma flow in the direction of the face pair normal is computed from R, the ratio of the ion saturation current collected by the face pair,[25]

$$\alpha \ln R = M_\parallel - M_\perp \cos(\theta + \pi), \qquad (21)$$

where $M_\parallel$ and $M_\perp$ are, respectively, the Mach numbers of flow in the direction along and perpendicular to the magnetic field, and α is a constant dependent upon the probe geometry. The face pair is oriented with normal at an angle, θ, to the magnetic field. In use, the central face pair is oriented with normal along the magnetic field, so that the other two pairs have their normals at ±45 degrees to the magnetic field. With this probe orientation, Eq. (21) yields the expressions

$$\alpha \ln R_0 = M_\parallel; \quad \alpha \ln R_{\pm45} = M_\parallel \mp \frac{1}{\sqrt{2}}M_\perp, \qquad (22)$$

where R_0 is the ratio of ion saturation current collected by the face pair oriented along the magnetic field, and $R_{\pm45}$ is the ratio for the other face pairs. Thus the six-faced Mach probe can directly measure flow in the direction along the magnetic field, and the perpendicular Mach number can be obtained by subtracting the expression for $\ln R_{+45}$ from the one for $\ln R_{-45}$ given in Eq. (22).

The radial profile of the azimuthal (poloidal) flow 3.5 ms after a 220 V rotation bias is applied ($t=9.5$ ms) is shown in Fig. 6(a). The magnetic field is 400 G. The normalized plasma density profile at this time is also shown for reference. Also shown is the flow profile before the bias is applied ($t=5.5$ ms). The flow, in the rotating plasma, begins to rise
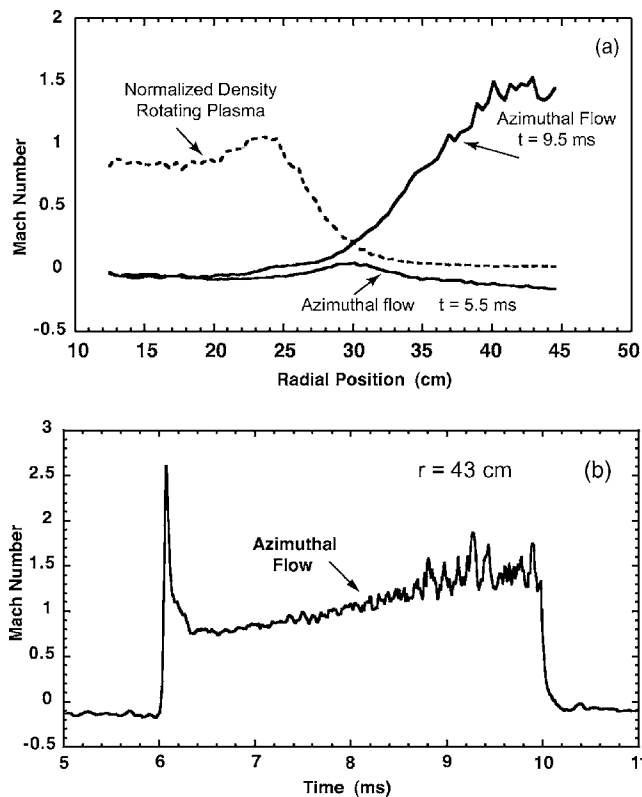
FIG. 6. (a) The radial profile of the azimuthal flow measured with a Mach probe is shown compared to the normalized plasma density measured with a triple probe for a steady-state rotating plasma ($t=9.5$ ms). The outer portions of the plasma rotate the fastest and the flow near the wall is supersonic. Also shown is the flow profile before the rotation bias is applied. Note the bias pulse reverses the flow in the outer regions of the plasma column. The bias is 220 V and the magnetic field is 400 G. (b) The temporal behavior of the flow at a radial position 43 cm from plasma center. At this location, a transient supersonic jet occurs when the bias pulse is first applied and then the flow becomes subsonic. The flow steadily increases until a steady state is achieved in the last millisecond before the bias pulse is terminated.
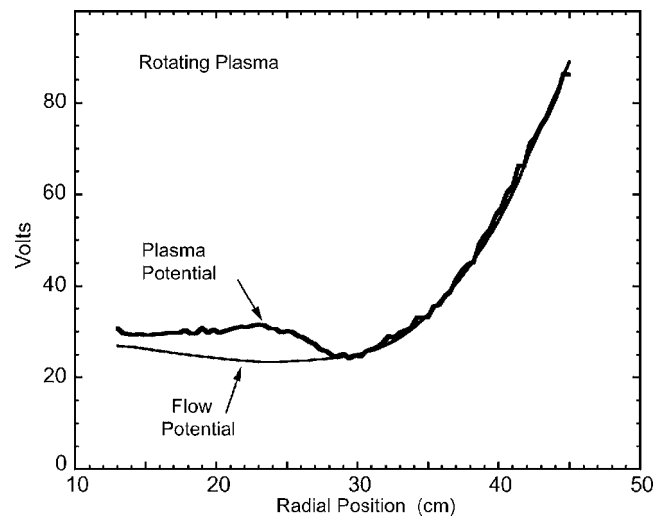

FIG. 7. The plasma potential derived from triple probe measurements is compared to the potential associated with the Mach probe measurements (labeled "flow potential"). The rotation bias is 220 V and the magnetic field is 400 G. The two potentials agree in the region of the plasma where pressure gradients are negligible.

near the outer edge of the plasma column, which is located near the edge of the cathode. This behavior likely arises because the cross-field ion current, which sets up the radial electric field associated with the azimuthal flow, terminates near the cathode edge. That is, ions drift across the magnetic field until they reach field lines connected to the edge of the cathode at which point electrons from the cathode flow along the magnetic field to neutralize their charge and complete the current in the bias circuit. The profile taken at $t=5.5$ ms in the so-called "nonrotating plasma" does have azimuthal flows associated with edge pressure gradients and gradients in the plasma potential, but they are small.

The temporal behavior of the flow at a radial location 43 cm from the center of the column with a 220 V bias pulse is shown in Fig. 6(b). At this radial location there is a transient, initial plasma response in which the measured flow is supersonic. This plasma jet is localized to a region near the chamber wall, and is short lived, lasting less than 100 μs. After the initial transient spike, the plasma flow drops below the sound speed and then steadily rises to a steady-state value slightly above the sound speed. Notice, also, that before the bias pulse is applied, there is a small (on the order of a tenth of the sound speed) azimuthal flow in the direction opposite the flow induced by the bias pulse.

The plasma electron temperature, T_e, and floating potential, ϕ_f, are measured using a triple probe. The plasma potential, ϕ_p, is derived from these measurements ($\phi_p = \phi_f + 4.02\,T_e$) and compared to measurements obtained from the Mach probe. To make the comparison, it is assumed the plasma rotation is due to $\mathbf{E} \times \mathbf{B}$ rotation so that the plasma flow can be related to an effective potential, ϕ_{mp},

$$v_{mp} = \frac{E}{B_0} = \frac{-1}{B_0}\frac{\partial \phi_{mp}}{\partial r}. \tag{23}$$

The potential, ϕ_{mp}, is that function whose radial derivative yields the flow velocity, v_{mp}, associated with the Mach probe measurement as indicated in Eq. (23). The Mach probe measurement yields a radial profile of the Mach number of the flow perpendicular to the magnetic field, $M_\perp(r)$, which, due to the radial insertion of the probe, is the Mach number of the azimuthal flow. Using Eq. (22), we obtain $M_\perp(r) = \alpha(R_{-45} - R_{+45})/\sqrt{2} = \alpha M_\theta(r)/\sqrt{2}$, where $M_\theta(r)$ is the unnormalized measurement of the azimuthal flow Mach number (the constant $\alpha/\sqrt{2}$ normalizes the measurement). The Mach number is the ratio between the azimuthal flow velocity and the local ion sound speed, $c_s(r)$, so that $v_{mp} = \alpha M_\theta(r)c_s(r)/\sqrt{2}$. The potential profile associated with the measured flow is thus

$$\phi_{mp} = -\frac{\alpha}{\sqrt{2}}B_0 \int_{r_1}^{r} M_\theta(r')c_s(r')dr'. \tag{24}$$

The radial profiles of the plasma potential obtained from triple probe data and the potential derived from Mach probe data are compared in Fig. 7 for the case of 220 V bias pulse, 3.5 ms after the pulse is initiated. The agreement is excellent in the regions where plasma pressure gradients are negli-
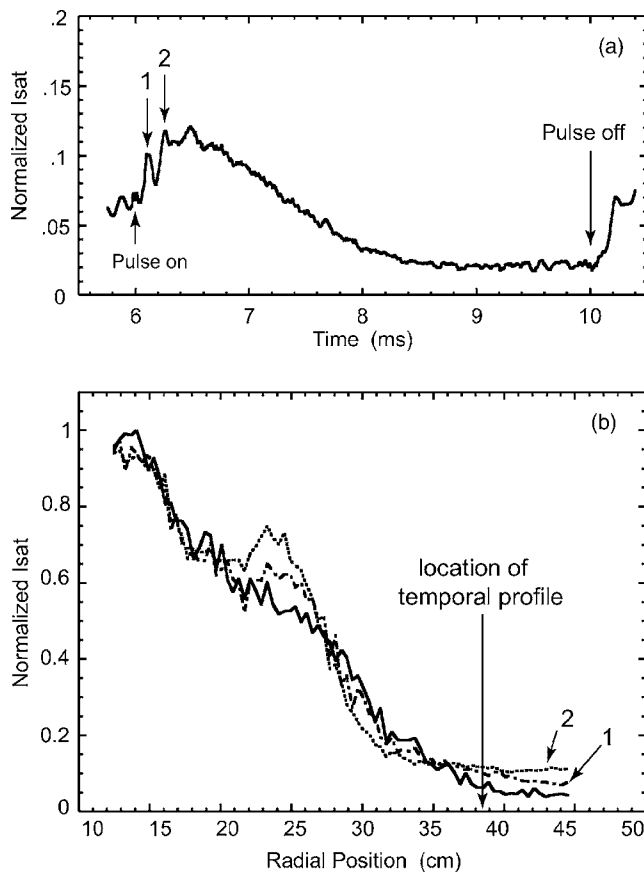
FIG. 8. (a) The temporal profile of ion saturation current at a radial position 38.5 cm from plasma center illustrating the oscillatory initial response and rapid increase of plasma density near the wall. After the initial increase, the density decays to a steady state with values below those of the nonrotating column. (b) The radial profiles associated with the two peaks in the initial oscillatory response to the bias pulse labeled "1" and "2" in panel (a). Notice the rapid rearrangement of the density profile in the region between 20 and 50 cm.

gible. This is precisely the region in which the two measurements should agree. The comparison of the two curves gives the value α, which is $\alpha = 1.5$. Since the Mach probe has a face size smaller than the ion gyroradius, this is a reasonable value for α.[24]

2. Initial response

When the bias pulse is applied, changes in the plasma occur rather quickly. In addition to the jet in plasma flow near the chamber wall, mentioned earlier, the entire plasma column moves radially, probably in response to the azimuthal electric field induced by the inductive response of the plasma column. This radial movement is oscillatory and strongly damped, lasting only a few cycles. This initial radial motion results in rapid changes in plasma density on field lines in the region between 20 and 50 cm, as shown in Fig. 8. Figure 8(a) displays the temporal behavior of the ion saturation current at a radial location of 38.5 cm and a rotation bias of 220 V and 400 G magnetic field. The initial oscillatory response is evident and the radial profiles corresponding to the two peaks marked "1" and "2" in Fig. 8(a) are shown in Fig. 8(b). Curve "1" represents the profile 100 μs after the
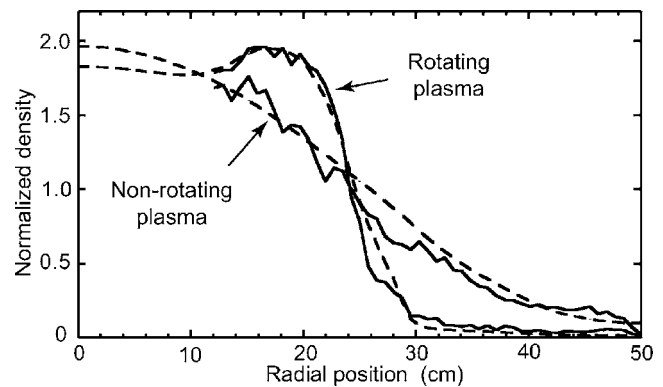

FIG. 9. Comparison of the measured plasma density profiles and model profiles in the rotating and nonrotating plasma columns. The solid curves are the measured density profiles and the dashed curves are model profiles for diffusion at the Bohm rate for the nonrotating column and at the classical rate for the rotating column. The model profiles are normalized to 2×10^{12} cm^{-3}. The end loss rate is increased from 800 to 950 s^{-1} in the model rotating plasma.

pulse is turned on and curve "2" represents the profile at 250 μs. Changes in the plasma profile occur on time scales much more rapid than the Bohm diffusion time scale. The Bohm diffusion coefficient in the region between 30 and 50 cm is about 5×10^4 cm^2/s, and the gradient scale length in this region is about 10 cm. Therefore, the time it takes plasma to diffuse across a distance equal to the gradient scale length is about 2 ms, whereas curve "2" indicates that the entire transient process is over in about 250 μs.

3. Density profiles in the rotating plasma

After the transient response, the density on field lines in the outer regions of the plasma column ($r > 30$ cm) decays, as shown in Fig. 8(a), to a steady-state value that is lower than in the nonrotating plasma. The solid curves in Fig. 9 are two measured radial plasma density profiles. One profile is obtained in the rotating plasma near the end of the 4 ms bias pulse, and the other profile is obtained in the nonrotating plasma, just before a 175 V rotation bias is applied. The dashed curves are predictions from diffusion models. The model density is normalized to a peak value of 2×10^{12} cm^{-3}. The model predictions are obtained by fitting the temporal evolution of the model beam source, $S_b(r,t)$ to the observed discharge current. The model density profile for the nonrotating plasma is then temporally evolved using Eq. (19), assuming Bohm diffusion applies. Measured temperature profiles are used to evaluate the Bohm diffusion coefficient. At the time the rotation bias pulse is applied, the diffusion coefficient is assumed to change from Bohm to classical. The model profiles are then evolved over the 4 ms duration of the bias pulse, using the classical diffusion coefficient,

$$D_C = \frac{kT_e \nu_{ei}}{m_e \Omega_e^2} = 1.29 \times 10^{-9} \frac{n}{T_e^{1/2}}, \qquad (25)$$

which is proportional to the density and the inverse square root of the temperature. The measured temperature profile
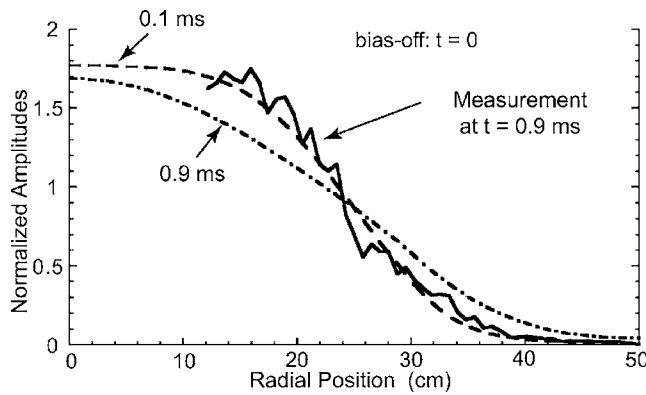
FIG. 10. The measured plasma density profile 0.9 ms after the rotation bias is terminated (solid curve) compared to the predictions of the Bohm diffusion model (dashed and dash-dot curves). The measured density profile best fits the 0.1 ms model profile, indicating that Bohm diffusion does not immediately resume upon termination of the bias pulse.

and the density profile from the previous time step are used to obtain D_C at the current time step.

The model plasma profile then evolves from the gentle-gradient, Bohm diffusion profile, just before the rotation bias is applied, into the steep gradient profile associated with classical diffusion. The development of the steep radial profile in the model takes less time than the total 4 ms duration of the bias pulse, which is consistent with observations. The radial profile of the beam electrons (the fast electrons emitted by the cathode) is the same for both the rotating and nonrotating plasmas, but the axial loss terms differ. The model predicts that the density in the plasma column should increase during the rotation pulse, due to the reduction of radial fluxes. However, measured density profiles do not show this increase. To get agreement between model predictions and observations, the end loss rate is increased from 800 to 950 s^{-1} during the rotation pulse.

The dramatically steeper density gradient observed in the rotating plasma results from decreased radial particle transport. In the model description of particle transport, the diffusion rate is suppressed globally. That is, classical diffusion is operative at all radial locations. An excellent fit to the data is obtained.

4. Profile recovery

The behavior of the plasma profile after the rotation bias is terminated is illustrated in Fig. 10. The solid curve is the measured density profile 0.9 ms after the rotation pulse is terminated. The diffusion model predicts that a steady-state profile should be recovered about 2.5 ms after bias termination. However, measured density profiles at times longer than 0.9 ms after bias termination are not available because the main plasma discharge is shut off at this time. The dashed curves in Fig. 10 are model profiles at two times (0.1 and 0.9 ms) after the rotation bias is terminated. The model profiles are obtained using the assumption that full Bohm diffusion is restored immediately upon termination of the rotation bias, although it should be noted that plasma rotation does not cease immediately upon termination of the bias. The decay time for plasma flow is about 50 μs. The measured pro-
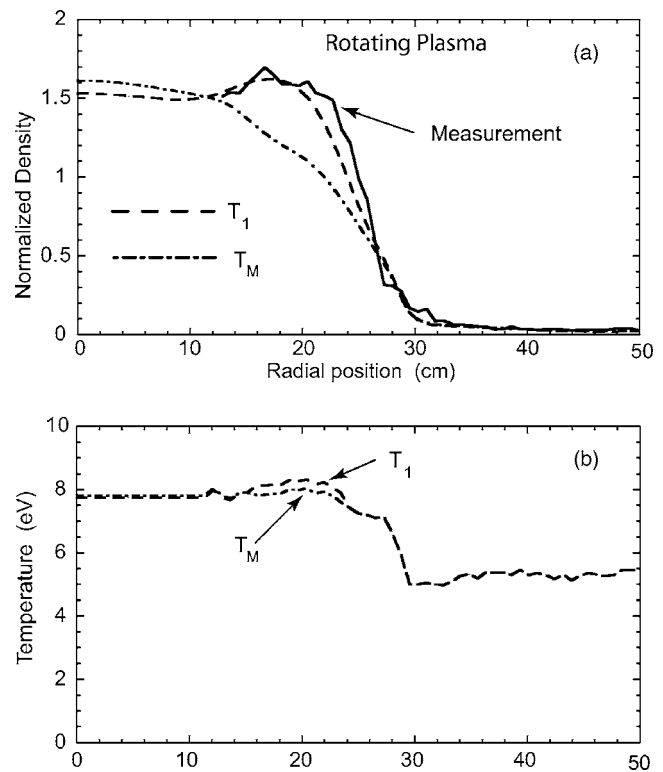

FIG. 11. (a) Comparison of two model profiles to the measured density profile of the rotating plasma (solid curve) near the end of the bias pulse. The model profile corresponding to the measured temperature T_M (dash-dot curve) does not fit the observed profiles as well as the model profile corresponding to T_1 (dashed curve). (b) The temperature profiles used to obtain the model density profiles produced by classical diffusion during the bias pulse. The profile T_1 is within the margin of error of the measured profile T_M.

file closely resembles the 0.1 ms model profile rather than the 0.9 ms profile. It appears that Bohm diffusion is not restored immediately upon termination of the bias pulse. A delay of up to 0.8 ms before Bohm diffusion is restored would be consistent with observation. This delay time is roughly comparable to the end loss time, L_c/c_s, which is 1.25 ms in the model calculations.

5. Temperature sensitivity of transport model

As mentioned previously, model density profiles are very sensitive to the electron temperature. The origin of this sensitivity is the very rapid change in the ionization rate of the bulk plasma in the temperature range of 5–10 eV, typical of LAPD plasmas. For example, the ionization rate changes from 3.67×10^{-10} cm^3/s at 8 eV to 4.57×10^{-10} cm^3/s at 8.5 eV, a 25% change![26] The effects of this sensitivity are illustrated in Fig. 11. Figure 11(a) shows two model profiles (the dashed and dash-dot curves) corresponding to two different temperature profiles shown in Fig. 11(b). The solid line in Fig. 11(a) is the measured density profile near the end of a 220 V bias pulse in a 400 G magnetic field. The model profiles correspond to times at the end of the rotation bias, and are obtained by the technique described in Sec. IV B 3. The temperature profile labeled T_M is the measured profile at a time corresponding to the middle of the bias pulse, and the profile labeled T_1 is a profile that gives a better fit to the

measured density profile. The largest difference between the two profiles is within the margin of error for the temperature measurement, less than 0.5 eV. The difference between the two profiles can be attributed entirely to the difference in the ionization rate. Since the profile labeled T_1 is within the margin of error of the measured profile, it is used in comparing model results to data.

Notice that the temperature profile measured during the bias pulse, Fig. 11(b), is elevated in the region $30 < r < 50$ cm, as compared to the profile measured in the nonrotating plasma [see Fig. 4(b) for an example]. Electrons are heated in the region of the plasma flow. The elevated temperature in this region ($30 < r < 50$ cm) results in a good fit between the measured density profile and the model profile.

6. Cross-field current

When the bias pulse is applied, the plasma is "spun up" by the torque exerted by the "$\mathbf{J} \times \mathbf{B}$" forces arising from radial currents. Radial currents are carried by ions. The ions move across the magnetic field in the direction of the electric field due to collisions with neutrals. In short, the currents arise from the Pederson[27] conductivity, σ_P, and the radial current, j_r, is related to the radial electric field, E_r, as $j_r = \sigma_P E_r$, with

$$\sigma_P = \frac{\omega_{p+}^2}{4\pi\Omega_+^2} \nu_{i0} = \frac{nec}{B_0} \frac{\nu_{i0}}{\Omega_+}, \tag{26}$$

where ν_{i0} is the ion-neutral collision frequency, and n is the plasma density. The ion-neutral collision frequency is related to the neutral density, n_0, and the ion velocity, v_i, as $\nu_{i0} = n_0 \sigma_0 v_i$, where σ_0 is the ion-neutral collision cross section (typically, about 5×10^{-15} cm^2). Thus the cross-field conductivity depends upon three temporally varying parameters: the plasma density, the ion velocity, and the neutral density. Figure 12 compares the temporal behavior, for the 220 and 125 V bias voltage cases, of the current flowing in the bias pulse circuit to the cross-field current density predicted using Eq. (26) for the conductivity. The ion velocity is taken to be the azimuthal plasma flow velocity and the plasma density is taken from triple probe measurements. Both flow velocity and density are evaluated at a single radial location (43 cm from column center). The temporal behavior of the neutral density is obtained from the calculation of the temporal evolution of the plasma density profiles for the rotating plasma, that is, the 4 ms time period when Bohm diffusion is turned off and classical diffusion prevails.

The comparison is for temporal behavior only as the amplitude of the current density is multiplied by an arbitrary factor to give a close fit to the total current profile. The same factor is used in both voltage bias cases. The similarity of the temporal behavior of the measured and modeled currents is a strong indication that the Pederson conductivity is indeed the source of the cross-field currents. If it is assumed that the "model current density" represents the current density at all radial and axial locations, the total current could be obtained by multiplying the current density by the area of the biased chamber wall (provided the numerical values of the neutral density and plasma density are known). The collecting area
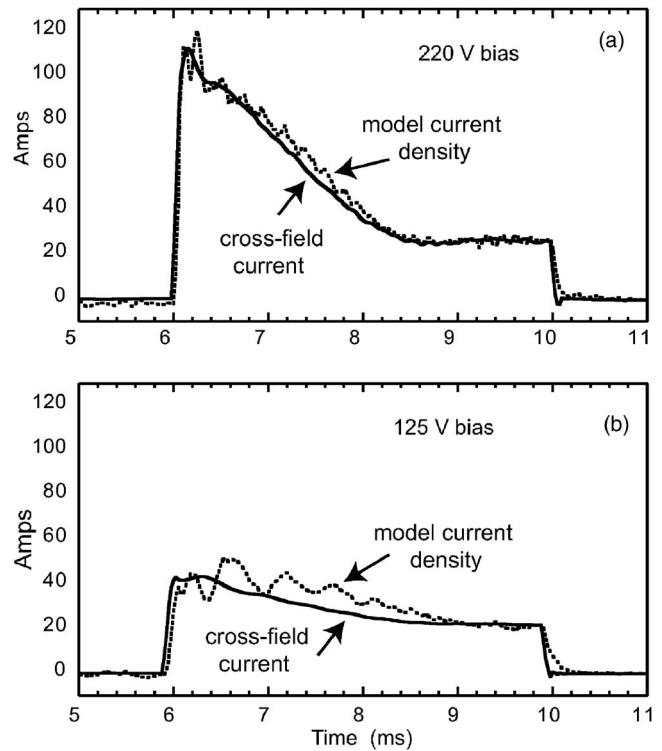

FIG. 12. The temporal behavior of the current flowing in the bias circuit is compared to the model Pederson current density computed from data obtained at a radial location 43 cm from the plasma center for two values of the bias voltage. The measured plasma flow and plasma density are combined with the model neutral density to obtain the curve labeled "model current density" and shown as a dotted curve in each panel. The solid curve is the measured current in the bias circuit. The amplitude of the model current density is adjusted to obtain the best fit to the total current flowing in the bias circuit.

of the chamber wall is about 30 m^2. The magnitude of the total current expected to arise from the Pederson conductivity can be estimated by assigning some expected values to the plasma density and neutral density. The ion-neutral collision frequency depends upon the ion velocity, which we take to be the plasma flow velocity (which is considerably larger than the ion thermal velocity). We have shown in Sec. IV B 1 that the measured plasma flow velocity is the $\mathbf{E} \times \mathbf{B}$ drift velocity. With $n = 1.6 \times 10^{11}$ cm^{-3} in the region outside the main plasma column and $n_0 = 2 \times 10^{12}$ cm^{-3}, the expected current density arising from the Pederson conductivity is about 16. E^2 $A/$m^2, where E is the electric field measured in kV/m. The E-squared dependence of this result arises from taking the ion velocity to be the $\mathbf{E} \times \mathbf{B}$ drift. The measured peak radial field in the 220 V bias case is about 500 V/m. Thus the expected total current is about 120 A, which is very close to the observed peak value of 110 A. The peak field for the 125 V bias case is proportionally smaller, about 290 V/m, so the expected peak current is 40 A, again close to the measured value.

7. Threshold for profile steepening

For a fixed bias pulse length, a threshold bias voltage must be exceeded in order to produce steep radial profiles. This phenomenon is illustrated in Fig. 13, which shows the
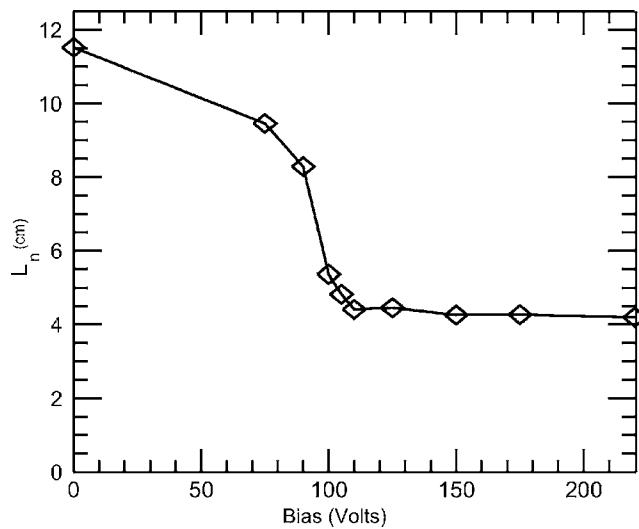
FIG. 13. Illustration of the existence of a threshold voltage for the transition from gentle to steep edge gradients. The gradient scale length, L_n, at the steepest slope in the radial density profile of the rotating plasma is plotted as a function of bias voltage for a bias pulse 4 ms in duration.

gradient scale length of the radial plasma profile at the location of the steepest slope, measured during application of the bias, as a function of bias voltage. The axial magnetic field is uniform with a strength of 400 G and the rotation bias pulse length is 4 ms for these measurements. An abrupt change in the gradient scale length occurs when the bias exceeds 75 V. This change may be related to the shear rate of the azimuthal velocity profile, dv_θ/dr. The shear rate becomes positive in the region of steepest density gradient in the nonrotating plasma ($r = 25 - 35$ cm) when the bias exceeds 75 V. At 100 V bias the shear rate is about 20 kHz in the steepest gradient region, and increases as the bias is increased, attaining a value of 100 kHz at 220 V bias. The drift frequency for the longest wavelength (lowest m number, $m=1$) azimuthal mode is about 5 kHz. The "step-function"-like behavior in the minimum gradient plot indicates a change in the global state of the plasma column once the threshold voltage is exceeded.

8. Global suppression of Bohm diffusion

In the model profile for the rotating plasma, Bohm diffusion is not suppressed over a particular radial range but at all radii. In particular, diffusion is not suppressed only in the region of flow shear. As illustrated in Fig. 14, model diffusion coefficients that are reduced in limited radial ranges do not produce density profiles that match the data. Figure 14(a) compares the density profile observed in a rotating plasma with a 175 V bias and 400 G magnetic field to two model profiles. The solid curve in Fig. 14(b) shows the plasma flow measured with a Mach probe and the dotted curve is the normalized flow shear obtained from a fit (the dashed curve) to the measured flow. The dashed curve, labeled "classical" in Fig. 14(a), is the model profile obtained using a classical diffusion coefficient at all radial locations. This model is called "global suppression" because there is no remnant of Bohm diffusion at any radius. The dashed curve, labeled "lo-
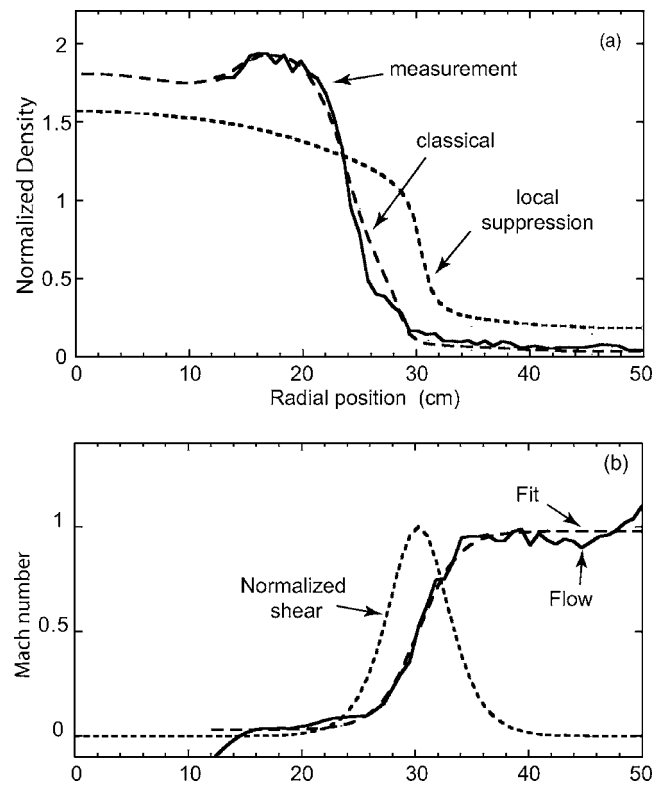
FIG. 14. (a) A comparison between the normalized density profile (solid curve) measured in the steady-state rotating plasma column for a rotation bias of 175 V to two model profiles. The dotted curve is the model profile for "global suppression" that refers to a model in which Bohm diffusion is replaced by classical diffusion at all radial locations. The dashed curve is the model profile for "local suppression" that refers to a model in which the diffusion coefficient is decreased in proportion to the value of the shear in the plasma flow. (b) The plasma flow data used in the "local suppression" model. The solid curve is the measured radial profile of the Mach number for azimuthal flow and the dotted curve is the normalized flow shear obtained from a fit to the Mach profile (dashed curve).

cal suppression," is the model profile using a Bohm diffusion coefficient reduced in proportion to the radial derivative of the flow, that is, the flow shear, namely, $D = D_B(1.0 - 0.95 \, \text{nfs})$, where nfs is the normalized flow shear. In the local suppression model, Bohm diffusion prevails in regions away from the shear layer. While the local suppression model produces a profile with a region of steep gradient, the profile is broader and lower than the observed profile. Although only one example of a local suppression model is shown, various models of locally suppressed diffusion were tried. The best fits to the data are obtained from the global suppression model.

9. Visual appearance of the plasma column

Figure 15 is a photograph of the LAPD plasma column taken from the end of the device looking toward the cathode. The photographs are taken with a charge coupled device (ccd) camera through a Pyrex window with a shutter speed of 10 μs, and show the plasma column with a 400 G magnetic field, before and after a 150 V bias is applied. The visual appearance of the column changes dramatically when the plasma is rotated. In the nonrotating plasma, Fig. 15(a), the plasma edge is ragged and structured in the azimuthal direc-
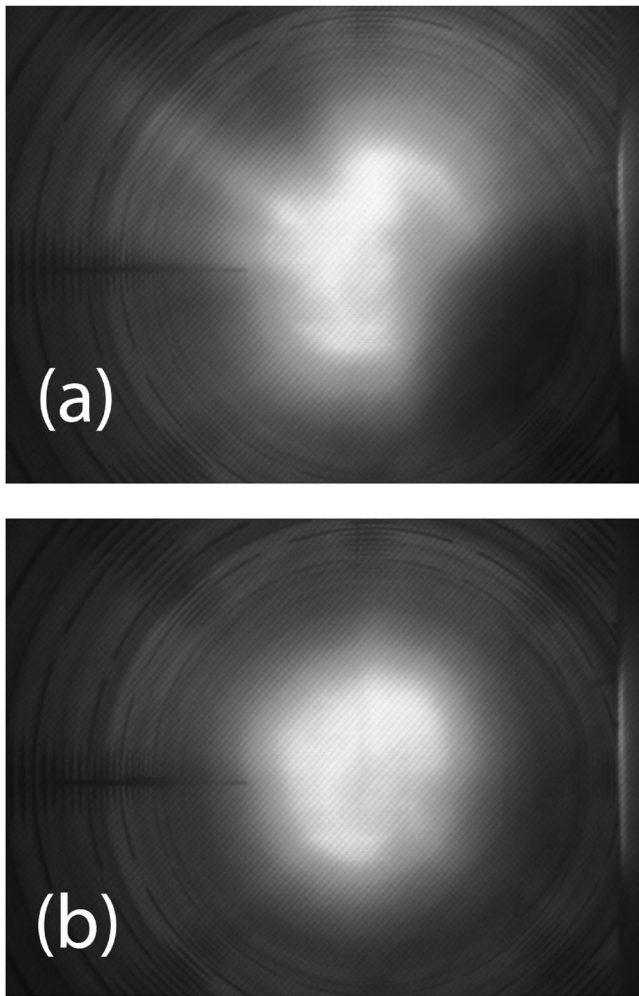
FIG. 15. A photograph of the plasma column as viewed from the end of the device, contrasting the appearance of the (a) nonrotating and (b) rotating plasma.

tion. In the rotating plasma, Fig. 15(b), the edge is smoother and more circular. From the photographic evidence, plasma rotation appears to suppress azimuthal structure in the plasma edge. This may imply that the modes associated with Bohm diffusion are modes with short azimuthal wavelengths (moderate to high m numbers). The global suppression of Bohm diffusion further suggests that these modes are global column modes.

V. CONCLUSIONS

The outer regions of the plasma column in the LAPD can be rotated, by biasing a section of the vacuum chamber wall positive with respect to the cathode. Plasma rotation results in dramatic suppression of cross-field (radial) particle transport, leading to steep gradients in the plasma density. The transition is very similar to the L to H mode transitions observed to occur in tokamaks. The simple linear magnetic geometry used in these experiments demonstrates that the suppression of radial particle transport by azimuthal rotation of the edge plasma can be achieved without the effects of field line curvature, trapped particles, or azimuthal asymmetries.

In the LAPD device, neutrals play an important role in the plasma rotation process because they allow the development of cross-field currents responsible for plasma rotation. The temporal behavior of the observed cross-field plasma current is consistent with the assumption that the perpendicular conductivity is due to ion-neutral collisions (Pedersen conductivity).

Plasma particle transport in the nonrotating plasma column is due to cross-field diffusion at the Bohm diffusion rate. Bohm diffusion results in plasma profiles with gentle edge gradients at low magnetic fields and steeper gradients at higher magnetic fields, although the behavior in the outer regions of the plasma column at high fields is aberrant.

Rotation of the outer edge of the plasma column results in greatly suppressed radial particle transport. Radial diffusion rates in the rotating plasma column are consistent with classical particle diffusion rates. Plasma rotation suppresses Bohm diffusion at all radial locations and not just in a layer isolated to the flow region or the region of flow shear. The global suppression of Bohm diffusion suggests that plasma flow effects the global structure and interaction of the turbulent plasma modes involved in Bohm diffusion, and this global change results in reduced radial transport.

APPENDIX: TRIDIAGONAL COEFFICIENTS

Consider the spatial part of Eq. (19),

$$-\frac{1}{r}\frac{\partial}{\partial r}rD_F\frac{\partial n}{\partial r} - \frac{1}{r}\frac{\partial}{\partial r}rD_Tn\frac{\partial \ln(T_e)}{\partial r} = S_bn_0 + R_pn_0n - \frac{n}{\tau_L},$$
(A1)

and let $D1=rD_F$ and $D2=rD_T\partial \ln(\mathrm{Te})/\partial r$. Then Eq. (A1) becomes

$$-\frac{1}{r}\frac{\partial}{\partial r}D1\frac{\partial n}{\partial r} - \frac{1}{r}\frac{\partial}{\partial r}nD2 = S_bn_0 + R_pn_0n - \frac{n}{\tau_L}.$$
(A2)

To implement a numerical scheme for evaluating the derivatives in (A2), write $r=j\Delta r$, where j is an integer. Then the first term becomes

$$\frac{1}{r}\frac{\partial h(r)}{\partial r} = \frac{1}{j(\Delta r)^2}\left[h\left(j+\frac{1}{2}\right) - h\left(j-\frac{1}{2}\right)\right],$$
(A3)

where $h(r)=D1\,\partial n/\partial r$ and $h(j\pm 1/2)=1/2[h(j\pm 1)+h(j)]$. Equation (A3) then becomes

$$\frac{1}{r}\frac{\partial}{\partial r}D1\frac{\partial n}{\partial r} = \frac{1}{j(\Delta r)^3}\left\{D1\left(j+\frac{1}{2}\right)[n(j+1)-n(j)]\right.$$

$$\left. - D1\left(j-\frac{1}{2}\right)[n(j)-n(j-1)]\right\}$$

$$= \frac{1}{2j(\Delta r)^3}\{[D1(j+1)+D1(j)]n(j+1)$$

$$- [D1(j+1)+2D1(j)+D1(j-1)]n(j)$$

$$+ [D1(j-1)+D1(j)]n(j-1)\}. \tag{A4}$$

Now consider the second term in (A2),

$$\frac{1}{r}\frac{\partial nD2}{\partial r}$$

$$= \frac{1}{j(\Delta r)^2}\left[n\left(j+\frac{1}{2}\right)D2\left(j+\frac{1}{2}\right) - n\left(j-\frac{1}{2}\right)D2\left(j-\frac{1}{2}\right)\right]$$

$$= \frac{1}{4j(\Delta r)^2}\{[D2(j+1)+D2(j)]n(j+1)+[D2(j+1)$$

$$- D2(j-1)]n(j)-[D2(j)+D2(j-1)]n(j-1)\}. \tag{A5}$$

The term on the right-hand side of (A2) is simply $R_p n_0 n(j) - n(j)/\tau_L$, so that the coefficients in the tridiagonal scheme are

$$a_j = \frac{-1}{2j(\Delta r)^2}\left[\frac{D1(j)+D1(j-1)}{\Delta r} - \frac{D2(j-1)+D2(j)}{2}\right],$$

$$b_j = \frac{1}{2j(\Delta r)^2}\left[\frac{D1(j+1)+2D1(j)+D1(j-1)}{\Delta r}\right.$$

$$\left. - \frac{D2(j+1)-D2(j-1)}{2}\right] + \frac{1}{\tau_L} - R_p n_0, \tag{A6}$$

$$c_j = \frac{-1}{2j(\Delta r)^2}\left[\frac{D1(j+1)+D1(j)}{\Delta r} + \frac{D2(j+1)+D2(j)}{2}\right].$$

To include the time dependence, write Eq. (19) as

$$\frac{\partial n}{\partial t} = -Tn + S_b n_0, \tag{A7}$$

where T is the tridiagonal matrix defined in Eq. (A6). Write the time derivative as $\partial n/\partial t = (n^k - n^{k-1})/\Delta t$, where the superscript denotes time step and Δt is the time interval. Equation (A7) then becomes

$$\frac{n^k}{\Delta t} = -Tn^k + S_b n_0 + \frac{n^{k-1}}{\Delta t}. \tag{A8}$$

Equation (A8) can be solved by the tridiagonal method at each time step k using the density at time step $k-1$ and by changing T and S using the prescription

$$b_j \rightarrow b_j + \frac{1}{\Delta t} \quad \text{and} \quad S_b n_0 \rightarrow S_b n_0 + \frac{n^{k-1}}{\Delta t}. \tag{A9}$$

[1]F. Wagner, G. Becker, K. Behringer *et al.*, Phys. Rev. Lett. **49**, 1408 (1982).

[2]R. J. Taylor, M. L. Brown, B. D. Fried, H. Grote, J. R. Liberati, G. J. Morlaes, P. Pribyl, D. Darrow, and M. Ono, Phys. Rev. Lett. **63**, 2365 (1989).

[3]R. J. Groebner, K. H. Burrell, and R. P. Seraydarian, Phys. Rev. Lett. **64**, 3015 (1990).

[4]J. Boedo, D. Gray, S. Jachmich, R. Conn, G. P. Terry, G. Tynan, G. Van Oost, and R. R. Weynants, TEXTOR Team, Nucl. Fusion **40**, 1397 (2000).

[5]G. R. Tynan, L. Schmitz, L. Blush *et al.*, Phys. Plasmas **1**, 3301 (1994).

[6]J. A. Boedo, P. W. Terry, D. Gray, R. S. Ivanov, R. W. Conn, S. Jachmich, and G. Van Oost, TEXTOR Team, Phys. Rev. Lett. **84**, 2630 (2000).

[7]R. R. Weynants and G. Van Oost, Plasma Phys. Controlled Fusion **35**, B177 (1993).

[8]P. H. Diamond, S.-I. Itoh, K. Itoh, and T. S. Hahm, Plasma Phys. Controlled Fusion **47**, R35 (2005).

[9]R. E. Waltz, G. D. Kerbel, J. Milovich, and G. W. Hammett, Phys. Plasmas **2**, 2408 (1995).

[10]K. C. Shiang, E. C. Krume, and W. A. Houlburg, Phys. Fluids B **2**, 1492 (1990).

[11]G. Furnish, W. Horton, Y. Kishimoto, M. LeBrun, and T. Tajima, Phys. Plasmas **6**, 1227 (1999).

[12]D. del-Castillo-Negrete, Phys. Plasmas **13**, 082308 (2006).

[13]W. Horton, Rev. Mod. Phys. **71**, 735 (1999).

[14]D. B. Melrose, *Instabilities in Space and Laboratory Plasmas* (Cambridge University Press, Cambridge, 1986), p. 227.

[15]H. Biglari, P. H. Diamond, and P. W. Terry, Phys. Fluids B **2**, 1 (1990).

[16]P. Brancher and J. M. Chomaz, Phys. Rev. Lett. **78**, 658 (1997).

[17]W. Gekelman, H. Pfister, Z. Lucky, J. Bamber, D. Leneman, and J. Maggs, Rev. Sci. Instrum. **62**, 2875 (1991).

[18]J. R. Peñano, G. J. Morales, and J. E. Maggs, Phys. Plasmas **7**, 144 (2000).

[19]J. E. Maggs and G. J. Morales, Phys. Plasmas **10**, 2267 (2003).

[20]D. R. Bates, A. E. Kingston, and R. W. P. McWhirter, Proc. R. Soc. London, Ser. A **267**, 297 (1962).

[21]R. K. Janev, W. D. Langer, K. Evans, Jr., and D. E. Post, Jr., *Elementary Processes in Hydrogen-Helium Plasmas Cross Sections and Rate Coefficients* (Springer-Verlag, Berlin, 1987).

[22]S. I. Braginskii, "Transport processes in a plasma," in *Reviews of Plasma Physics*, edited by M. A. Leontovich (Consultants Bureau, New York, 1965), Vol. 1, p. 205.

[23]H. Ramachandran, G. J. Morales, and B. D. Fried, Phys. Fluids B **5**, 872 (1993).

[24]P. Helander and D. J. Sigmar, *Collisional Transport in Magnetized Plasmas* (Cambridge University Press, Cambridge, 2002).

[25]T. Shikama, S. Kado, A. Okamoto, S. Kajita, and S. Tanaka, Phys. Plasmas **12**, 044505 (2005).

[26]R. K. Janev, W. D. Langer, K. Evans, Jr., and D. E. Post, Jr., *Elementary Processes in Hydrogen-Helium Plasmas Cross Sections and Rate Coefficients* (Springer-Verlag, Berlin, 1987), pp. 91 and 263.

[27]*Auroral Plasma Physics*, edited by G. Paschmann, S. Haaland, and R. Treumann (Kluwer Academic, Dordrecht, 2003), p. 44.